Electronic Supplementary Material (ESI) for Nanoscale.
This journal is © The Royal Society of Chemistry 2019

Supporting Information for

Combining Co_3S_4 and $Ni:Co_3S_4$ nanowires as efficient catalysts for overall water splitting: an experimental and theoretical study

Shasha Tang,[1] Xing Wang,[2] Yongqi Zhang,[1] Marc Courté,[1] Hong Jin Fan,[1] and Denis Fichou.[1,3]*

[1] School of Physical and Mathematical Sciences, Nanyang Technological University, 637371, Singapore

[2] Institute for Chemical and Bioengineering, ETH Zurich, Vladimir Prelog Weg 1, 8093 Zurich, Switzerland

[3] Sorbonne Université, CNRS, Institut Parisien de Chimie Moléculaire (UMR 8232), 4 place Jussieu, 75005 Paris, France.

*Corresponding Author: E-mail: denisfichou@ntu.edu.sg

1. Experimental Section

a. Synthesis of Cobalt-based Materials

The Co_3O_4 nanowire was synthesized on commercial nickel foam by hydrothermal method. A piece of pressed Ni foam was sonication cleaned with de-ionized water and ethanol. Polytetrafluoroethylene tape was utilized to protect the backside of Ni foam from solution contamination. Afterward, the Ni foam was immersed in Teflon liners containing 60 mL de-ionized water of 2 mmol cobalt nitrate, 4 mmol ammonium fluoride, 10 mmol urea. Then, the Teflon liners were put in the stainless steel autoclave and maintained at 120^{o}C for 4 hours. After hydrothermal reaction, the sample was rinsed with de-ionized water and ethanol several times. The dark grey Ni foam turned pink, suggesting the formation of cobalt-based material. Subsequently, the sample was annealed at 300^{o}C for 1 hour in air. This turned the pink Ni foam black, suggesting the conversion from cobalt-based precursor to Co_3O_4. The average mass loading of Co_3O_4 is 2.5 mg cm^{-2}.

To synthesize Co_3S_4, the above Co_3O_4 sample underwent an ion exchange reaction in another hydrothermal treatment. The backside of the above sample was again covered with polytetrafluoroethylene tape and then sealed in Teflon-lined stainless steel autoclave liners containing 60 mL of deionized water of 300 mg $Na_2S.6H_2O$. The autoclave was heated at 160^{o}C for 6 hours. After cooling down naturally, the sample was rinsed several times with deionized water and ethanol.

To obtain nickel doped cobalt-based materials, 0.1 mmol nickel nitrate was added in the first hydrothermal process. Other heat treatment and sulfurization process were the same as above. Also, we collected the precipitated pink powders after the first hydrothermal reaction and washed them with de-ionized water and ethanol by centrifugation. After drying at 60^{o}C for 5 hours, the powder sample was annealed under above conditions and collected as Ni:Co_3O_4 powder. After drying at 60°C for 5 hours, the powders were annealed at 300°C for 1 hour in air. Then, these Ni:Co_3O_4 powders were converted to Ni:Co_3S_4 under the similar ion exchange condition as above. The Ni:Co_3O_4 and Ni:Co_3S_4 powders are completely dissolved in pure nitrate acid and used to perform the ICP-OES characterizations.

b. Material Characterization

The morphology and size of cobalt-based materials were characterized using field emission scanning electron microscopy (FESEM, FEI SIRION) and transmission electron microscopy (TEM, JEOL-2010 HR & UHR and JEOL-2100F with UHR Configuration). The chemical composition of cobalt-based materials was confirmed by X-ray diffraction (XRD, 6000 Shimadzu) and a Thermo Fischer iCAP 6000 series inductively coupled plasma optical emission spectrometer (ICP-OES).The chemical valence states of cobalt-based sulfide materials were detected by X-ray photoelectron spectroscopy (XPS, PHI 5700).

c. Electrochemical Characterization

Electrochemical testing was conducted in a three-electrode glass configuration via a Zahner-Zennuim electrochemical workstation. The samples grown on Ni foam were used as working electrodes, a platinum foil/carbon rod as the counter electrode, and an Ag/AgCl (3.0 M KCl) electrode as the reference. All electrodes were immersed into the 1 M KOH electrolyte, and the electrolyte was bubbled with high purity O_2 gas for 15 min before the test. All the tests were conducted at room temperature. Before any measurements were performed, cyclic voltammetry from 0 to 0.8 V at 50 mV s^{-1} were carried out 20 cycles, which is an activation process to stabilize the current and detach any impurity formed on the surface of the electrode. Then, the linear sweep voltammetry (LSV) tests were performed at 2 mV s^{-1} for the polarization curves. All data were dealt with iR-compensation by the current-interrupt method. The main point of this method is to consider uncompensated cell resistance (R). Generally, the obtained potential is corrected by subtracting ohmic drop (iR), where i is the current related to the potential. Tafel plots were derived from the above LSV curves by fitting the data to the equation $\eta = a + b\log(j)$, where η is the *iR*-compensated overpotential, a is the Tafel constant, b is the Tafel slope, and j is the current density. The stability was investigated at fixed current densities (10, 30, and 50 mA cm^{-2}) by chronopotentiometry. The current density was calculated based on the geometric area of the electrode. The Faradaic efficiency was estimated using the volumetric method. In all measurements, Ag/AgCl (3.0 M KCl) electrode was used as the reference, which has the potential of 0.210 V *vs.* RHE. Potentials obtained in this study were calibrated against the reversible

hydrogen electrode (RHE) reference by the following equation: E (V *vs.* RHE) = E (V *vs.* Ag/AgCl) +0.059 pH + E (Ag/AgCl *vs.* RHE). In our study, η_{10} is the iR-compensated overpotential which can achieve a current density of 10 mA cm^{-2}.

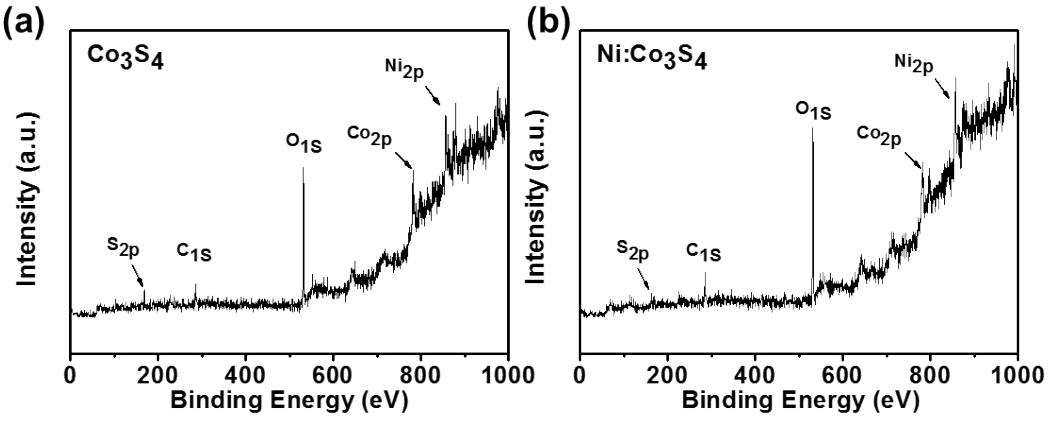

Figure S1 XPS full survey results of the Co_3S_4 and Ni:Co_3S_4 samples.

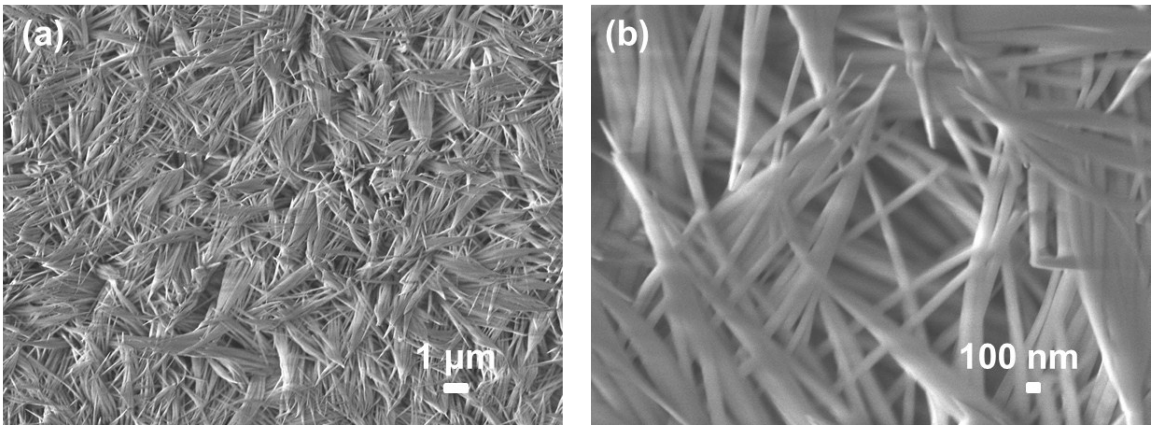

Figure S2 Different magnification SEM images of the Co_3O_4 precursor after the first hydrothermal method.

Table S1 Atomic ratio of Ni:Co_3O_4 and Ni:Co_3S_4 materials determined by ICP-OES measurements.

Material	**Ni:Co_3O_4**		**Ni:Co_3S_4**	
Element	Ni	Co	Ni	Co
Units	ppm	ppm	ppm	ppm
Average	**0.3085**	**3.069**	**0.0700**	**0.6880**
Stddev	0.0015	0.011	0.0002	0.0008
%RSD	0.4893	0.3435	0.2291	0.1116
Average atom ration of Ni:Co	**10.05%**		**10.17%**	

Table S2 Summary of OER and HER performance of the as-prepared Co-based catalysts in 1.0 M KOH electrolyte.

Catalyst	Overpotential @10 mA cm^{-2} (mV)	Tafel slope (mV dec^{-1})	Overpotential @10 mA cm^{-2} (mV)	Tafel slope (mV dec^{-1})
	OER		HER	
Co_3O_4	371	69	221	110
Co_3S_4	283	66	218	134
Ni:Co_3O_4	348	74	222	93
Ni:Co_3S_4	293	65	199	91

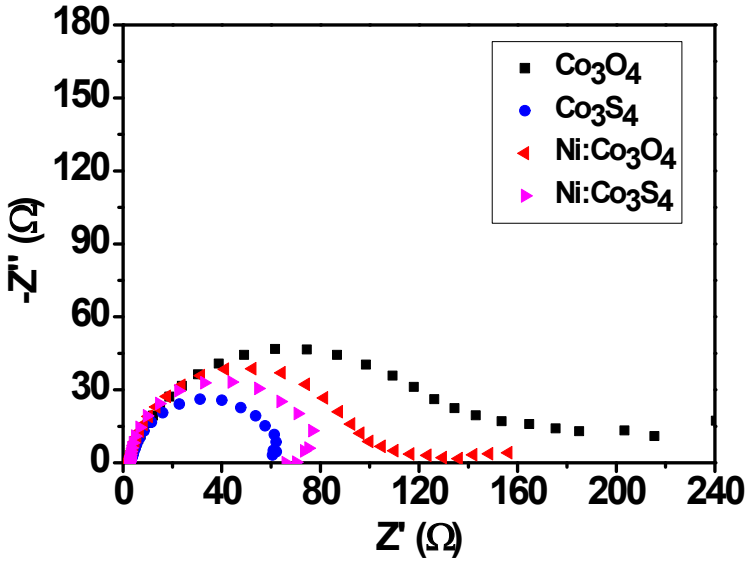

Figure S3 Nyquist plots of cobalt-based catalysts in the frequency range from 100 kHz to 100 H. Impedance tests are performed in a three-electrode glass configuration in 1.0 M KOH electrolyte. These catalysts are used as working electrodes, a platinum foil as counter electrode, and an Ag/AgCl (3.0 M KCl) electrode as the reference electrode.

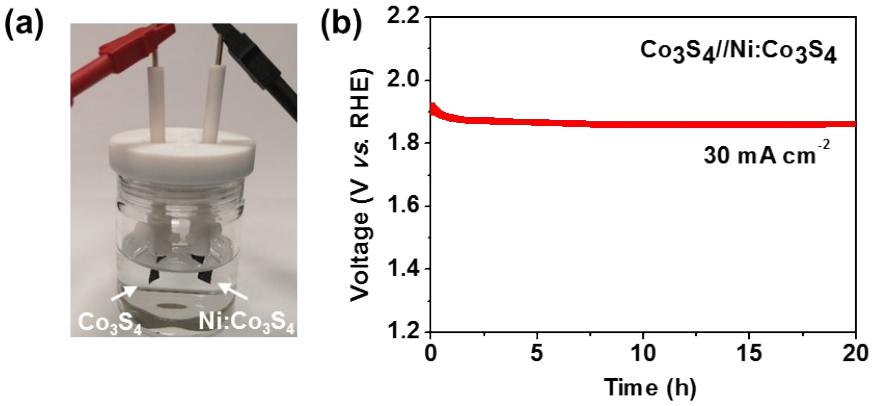

Figure S4 (a) Overall water splitting tests in a two-electrode configuration with 1.0 M KOH as the electrolyte, where Co_3S_4 acts as the OER electrode and $Ni:Co_3S_4$ as the HER electrode (denoted as Co_3S_4//$Ni:Co_3S_4$). (b) Stability test of above Co_3S_4//$Ni:Co_3S_4$ system under a constant current density of 30 mA cm^{-2} (geometric area) for 20 hours.

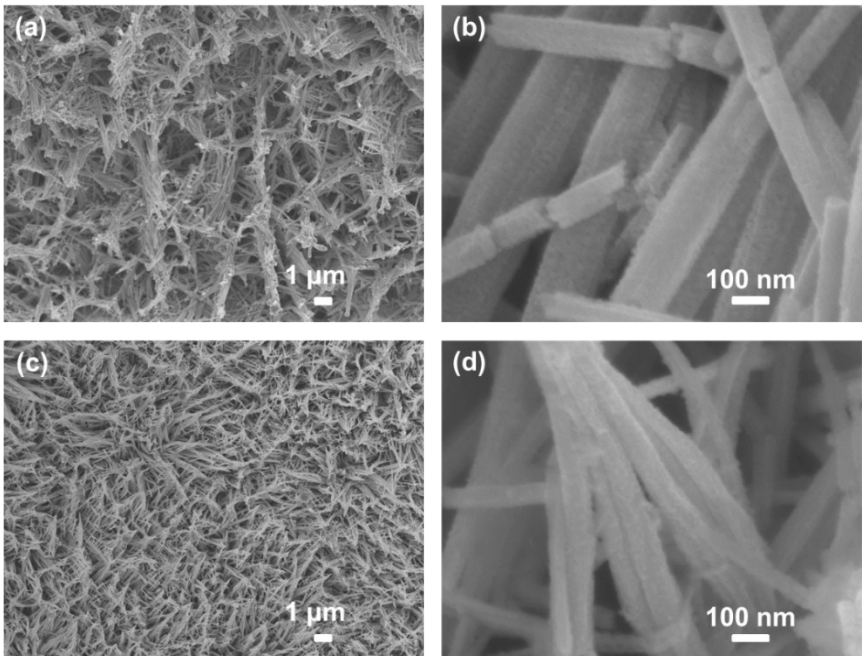

Figure S5 SEM images of the morphology of (a-b) Co_3S_4 nanowires (act as the OER electrode) and (c-d) Ni:Co_3S_4 nanotubes (act as the HER electrode) after stability test for overall water splitting in 1.0 M KOH electrolyte under a constant current density of 30 mA cm^{-2} for 20 hours.

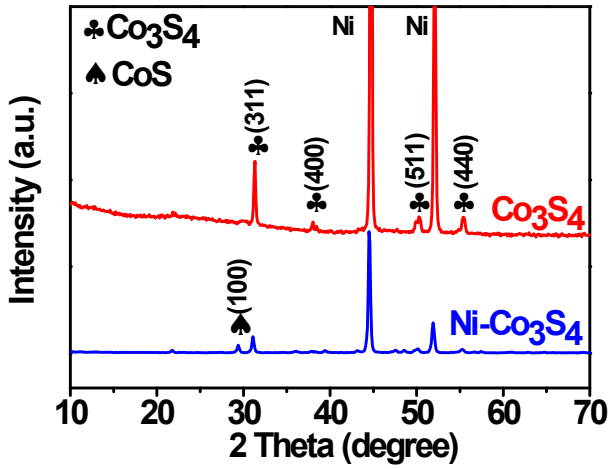

Figure S6 XRD patterns of Co_3S_4 (red line) and Ni:Co_3S_4 (blue line) after stability test for overall water splitting in 1.0 M KOH electrolyte under 30 mA cm^{-2} for 20 hours. ♣ denotes the peaks corresponding to the Co_3S_4 (JCPDS 19-0367), and ♠ can be indexed to the CoS (JCPDS 70-2864).

Table S3 Comparison of the OER performance of as-prepared our catalysts and reported Co-related catalysts

Catalyst	Overpotential @10mA/cm^2(mV)	Tafel slope (mV dec^{-1})	Substrate	Electrolyte
Co_3S_4 (our work)	283	66	Ni foam	1.0 M KOH
Ni: Co_3S_4 (our work)	293	65	Ni foam	1.0 M KOH
CoN[7]	290	70	Ni foam	1.0 M KOH
Co_4N[8]	257	44	Carbon cloth	1.0 M KOH
Co_2B[9]	380	45	Powder	3.0 M KOH
CoS[10]	306	72	Carbon paper	1.0 M KOH
$NiCo_2S_4$[11]	260	40	Ni foam	1.0 M KOH
IrO_2[11]	340	72.5	Ni foam	1.0 M KOH
S-Co/CNS[12]	320	52.3	Powder	1.0 M KOH

Table S4 Summary of the electrochemical activities of the catalytic electrodes for overall water splitting

Catalyst	Votalge@10mA/cm^2	Durability	Substrate	Electrolyte
Co_3S_4 // Ni:Co_3S_4 (our work)	1.70 V	40 h	Ni foam	1.0 M KOH
Co_2B // Co_2B[9]	1.81 V	-	Powder	3.0 M KOH
Co-S // Co-S[10]	1.74 V	2 h	Carbon paper	1.0 M KOH
$NiCo_2S_4$ NW // $NiCo_2S_4$ NW[11]	1.63 V	50 h	Ni foam	1.0 M KOH
Ni_3S_4 // Ni_3S_4[11]	1.73 V	-	Ni foam	1.0 M KOH
NiS // NiS[13]	1.64 V	35 h	Ni foam	1.0 M KOH
$NiCo_2S_4$ // $NiCo_2S_4$[14]	1.68 V	10 h	Carbon cloth	1.0 M KOH
$NiCo_2O_4$ // $NiCo_2O_4$[14]	1.98 V	-	Carbon cloth	1.0 M KOH
$CoNi(OH)_x$ // NiN_x[15]	1.65 V	-	Cu foil	1.0 M KOH

2. Computational Models and Methods

Spin-polarized DFT calculations have been performed using the full-potential all-electron code FHI-aims[1] at the level of the generalized gradient approximation (GGA) in the Perdew-Burke-Ernzerhof (PBE) parameterization.[2] A pre-constructed high-accuracy all-electron basis set of numerical atomic orbitals was employed, as provided by the FHI-aims default option. Structural optimization was performed with a tolerance of 10^{-3}eV/Å. All geometries and energies reported herein correspond to the optimal spin state for each system. Co_3O_4 adopts the normal spinel structure with Co^{2+} (Co^{3+}) ions located in the tetrahedral (octahedral) sites of the face centered cubic lattice formed by O^{2-} anions. The effects of the coverage on the catalytic activities have been discussed by García-Mota *et al.*[3] and Zhang *et al.*[4] for the cobalt oxide systems. Surfaces with coverage of O/OH are reported to be more active than the clean surface. Therefore, half-monolayer OH covered surface model is used for the oxygen-poor A termination. For the oxygen-rich B termination, a clean surface model is used.

In this study, the adsorption energy (ΔE_{ads}) for H*, OOH*, O*, and OH* were calculated by the following equations:

$$\Delta E_{H^*} = E(H^*) - E(^*) - 1/2E_{H2} \quad (1)$$

$$\Delta E_{OOH^*} = E(OOH^*) - E(^*) - (2E_{H2O} - 3/2E_{H2}) \quad (2)$$

$$\Delta E_{O^*} = E(O^*) - E(^*) - (E_{H2O} - E_{H2}) \quad (3)$$

$$\Delta E_{OH^*} = E(OH^*) - E(^*) - (E_{H2O} - 1/2E_{H2}) \quad (4)$$

Where * and X* denotes surfaces and adsorbed X species, respectively. The energies of isolated molecules (H_2, H_2O, O_2) were computed in an orthorhombic cell of dimensions 10 Å ×11 Å ×12 Å. The OER energy profile were constructed based on the model developed by Nørskov.[5] In the scheme, the OER is assumed to involve four elementary reaction steps and each step involves electron transfer of an electron to the electrode and a proton to water:

$$H_2O + * \rightarrow OH^* + H^+ + e^- \quad (5)$$

$$HO^* \rightarrow O^* + H^+ + e^- \quad (6)$$

$O^* + H_2O \rightarrow OOH^* + H^+ + e^-$ (7)

$OOH^* \rightarrow O_2 + H^+ + e^-$ (8)

Based on the computational hydrogen electrode model,[5] the free energy change along the OER processes (ΔG_n, n = 1-4) at standard conditions can be derived as:

$\Delta G_1 = \Delta G_{OH^*}$ (9)

$\Delta G_2 = \Delta G_{O^*} - \Delta G_{OH^*}$ (10)

$\Delta G_3 = \Delta G_{OOH^*} - \Delta G_{O^*}$ (11)

$\Delta G_4 = 4.92 - \Delta G_{OOH^*}$ (12)

Then the theoretical overpotentials (η) for OER can be calculated using the equations:

$\eta = \max \{\Delta G_1, \Delta G_2, \Delta G_3, \Delta G_4\}/e - 1.23$ (V) (13)

The adsorption energy of a single H atom (ΔG_{H^*}) is usually considered as an effective descriptor for evaluating the hydrogen evolution reaction (HER) activity over a given system.[6] Generally, the smaller (ΔG_{H^*}) absolute value, the better the HER activity. ΔG_{H^*} can be calculated by:

$\Delta G_{H^*} = \Delta E_{H^*} + \Delta ZPE - T\Delta S$ (14)

Where ΔE_{H^*} is the binding energy, ΔZPE is the zero-point energy (ZPE) difference and ΔS is the entropy change of H*. The ZPE of H atom in different state (gas and adsorbed state) are very similar, thus ΔZPE is close to zero. The entropy of hydrogen in absorbed state is negligible, and TΔS is calculated based on the entropy of H_2 in the gas phase. TΔS is determined to be -0.21 eV.

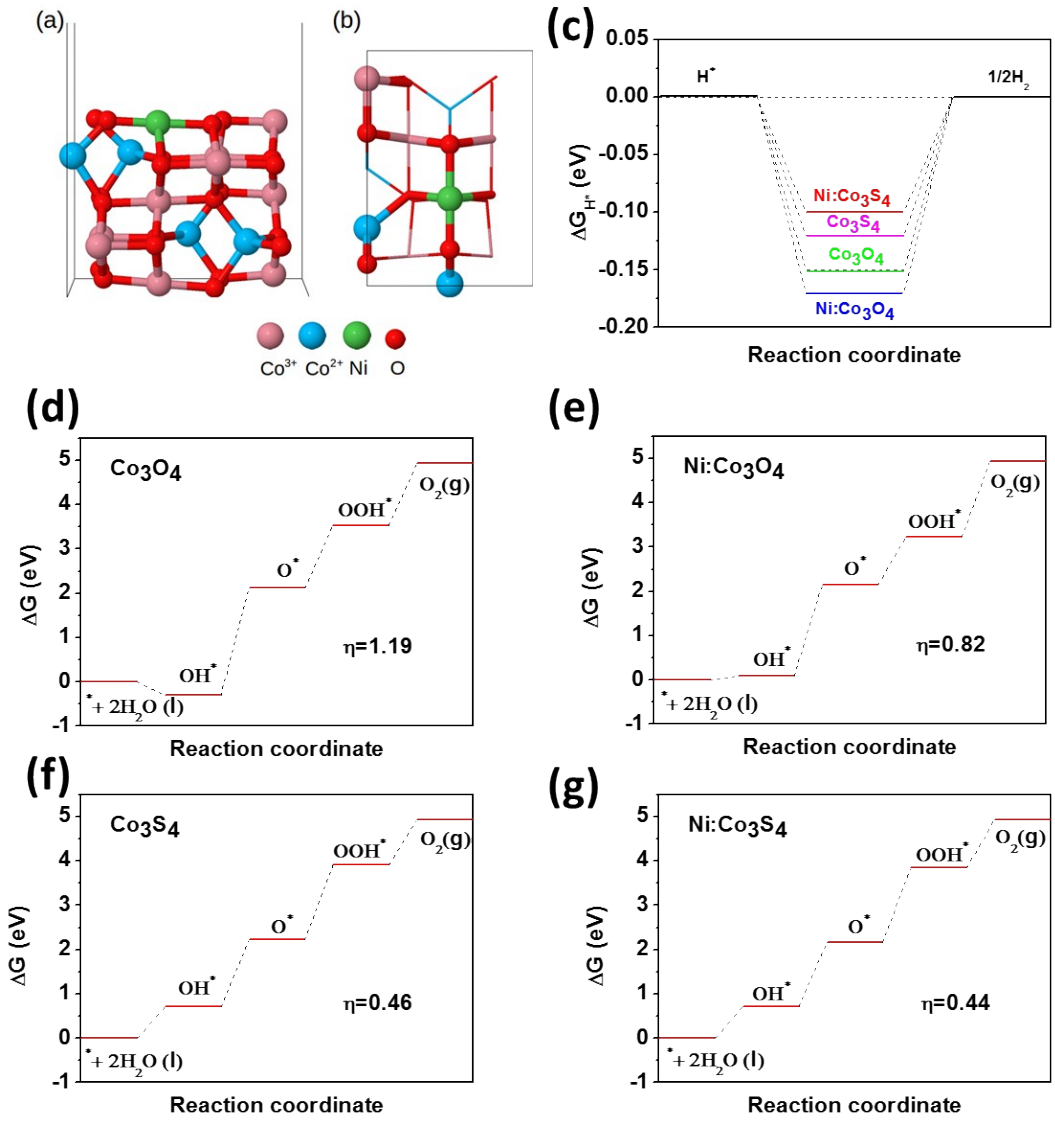

Figure S7 (a) Side view and (b) top view of the B termination of Ni:Co_3O_4 (110) surface. In the top view of the structure, the atoms at the top layer are illustrated by ball-and-stick models, and the rest of the atoms are given by line models. $Co^{3+,}$ Co^{2+}, Ni, and O atoms are shown in pink, blue, green and red, respectively. (c) Calculated free energy diagram for the HER process on the B termination of four catalysts. Calculated free energy diagram for the OER process on the B termination of Co_3O_4 (d), Ni:Co_3O_4 (e), Co_3S_4 (f), and Ni:Co_3S_4 (g) and the corresponding theoretical overpotential.

3. References

1. V. Blum, R. Gehrke, F. Hanke, P. Havu, V. Havu, X. Ren, K. Reuter and M. Scheffler, *Computer Physics Communications*, 2009, **180**, 2175-2196.
2. J. P. Perdew, K. Burke and M. Ernzerhof, *Physical Review Letters*, 1996, **77**, 3865-3868.
3. M. García-Mota, M. Bajdich, V. Viswanathan, A. Vojvodic, A. T. Bell and J. K. Nørskov, *The Journal of Physical Chemistry C*, 2012, **116**, 21077-21082.
4. P. Zhang, Y. Dong, Y. Kou, Z. Yang, Y. Li and X. Sun, *Catalysis Letters*, 2015, **145**, 1169-1176.
5. J. K. Nørskov, J. Rossmeisl, A. Logadottir, L. Lindqvist, J. R. Kitchin, T. Bligaard and H. Jónsson, *The Journal of Physical Chemistry B*, 2004, **108**, 17886-17892.
6. J. K. Nørskov, T. Bligaard, A. Logadottir, J. R. Kitchin, J. G. Chen, S. Pandelov and U. Stimming, *Journal of The Electrochemical Society*, 2005, **152**, J23.
7. Y. Zhang, B. Ouyang, J. Xu, G. Jia, S. Chen, R. S. Rawat and H. J. Fan, *Angewandte Chemie*, 2016, **55**, 8670-8674.
8. P. Chen, K. Xu, Z. Fang, Y. Tong, J. Wu, X. Lu, X. Peng, H. Ding, C. Wu and Y. Xie, *Angewandte Chemie*, 2015, **54**, 14710-14714.
9. J. Masa, P. Weide, D. Peeters, I. Sinev, W. Xia, Z. Sun, C. Somsen, M. Muhler and W. Schuhmann, *Advanced Energy Materials*, 2016, **6**, 1502313.
10. J. Wang, H. X. Zhong, Z. L. Wang, F. L. Meng and X. B. Zhang, *ACS Nano*, 2016, **10**, 2342-2348.
11. A. Sivanantham, P. Ganesan and S. Shanmugam, *Advanced Functional Materials*, 2016, **26**, 4661-4672.
12. M. Al-Mamun, Z. Zhu, H. Yin, X. Su, H. Zhang, P. Liu, H. Yang, D. Wang, Z. Tang, Y. Wang and H. Zhao, *Chemical communications*, 2016, **52**, 9450-9453.
13. W. Zhu, X. Yue, W. Zhang, S. Yu, Y. Zhang, J. Wang and J. Wang, *Chemical communications*, 2016, **52**, 1486-1489.
14. D. Liu, Q. Lu, Y. Luo, X. Sun and A. M. Asiri, *Nanoscale*, 2015, **7**, 15122-15126.
15. S. Li, Y. Wang, S. Peng, L. Zhang, A. M. Al-Enizi, H. Zhang, X. Sun and G. Zheng, *Advanced Energy Materials*, 2016, **6**, 1501661.